Available online at www.sciencedirect.com

ScienceDirect

Ceramics International 40 (2014) 3315–3324

CERAMICS INTERNATIONAL

www.elsevier.com/locate/ceramint

Chemical control on the size and properties of nano $NiFe_2O_4$ synthesized by sol–gel autocombustion method

T. Prabhakaran, J. Hemalatha*

Advanced Materials Lab, Department of Physics, National Institute of Technology, Tiruchirappalli, India

Received 30 April 2013; received in revised form 1 September 2013; accepted 23 September 2013
Available online 29 September 2013

Abstract

Nickel ferrite nanoparticles have been synthesized by sol–gel auto combustion route. The significant role played by nitric acid added to the precursor solution in controlling the reaction rate phase purity, crystallinity, crystallite size, thermal and magnetic properties of nanoparticles was explored and reported. Also, the influence of annealing on the properties were studied. Samples of average crystallite size ranging from 10 nm to 40 nm have been obtained by controlling the HNO_3 concentration and by increasing the annealing temperature. The size-dependent structural, thermal and magnetic properties were investigated and reported. The Hopkinson peak was observed for all the crystalline samples near the Curie temperature. The highest value 47.3 emu/g of saturation magnetization was obtained for the sample prepared with higher concentration (6 mol/L) of HNO_3.

Keywords: A. Sol–gel Processes; B. X-ray methods; C. Magnetic properties; C. Thermal Properties; D. Ferrites

1. Introduction

Study of spinel ferrites has gained enormous importance in recent years because of the technologically significant electrical and magnetic properties of ferrites and their broad practical applications in magnetic recording media, magnetic fluids for the storage and retrieval of information, magnetic resonance imaging (MRI) enhancement, catalysis, magnetically guided drug delivery, sensors, pigments etc. [1,2]. The structural formula of spinel-type ferrites can be written as $(M_{1-\lambda}^{2+}\ Fe_{\lambda}^{3+})[M_{\lambda}^{2+}\ Fe_{2-\lambda}^{3+}]O_4^{2-}$, where parentheses and square brackets denote cation sites of tetrahedral (A) and octahedral [B] coordination, respectively. λ, which is determined by the preparation process, represents the degree of inversion defined as the fraction of the (A) sites occupied by Fe^{3+} cations [3]. Nickel ferrite (NFO) of molecular formula $NiFe_2O_4$, with an inverse spinel structure shows ferrimagnetism that originates from the divalent Ni^{2+} and trivalent Fe^{3+} cation distribution in A and B sites. In $NiFe_2O_4$, the divalent Ni^{2+} ions are in B sites, and the trivalent Fe^{3+} ions are equally divided between A and B sites. The moments of Fe^{3+} ions in B sites are antiparallel to the moments of Fe^{3+} ions in A sites. Therefore, the moments of Fe^{3+} ions cancel and the net moment is simply that of Ni^{2+} ion which is 2 μB [4].

The preparation and characterization of NFO in nano scale would allow investigating the fundamental aspects of anomalous properties different from those of bulk properties which is of primary importance for continued advancement and practical applications. There are plenty of methods, such as sol–gel [5], mechanosynthesis [6], co-precipitation [7], and microemulsion [8], sol–gel combustion [9], hydrothermal treatment [10,11], ball milling [12], and electrospinning [13], available to synthesize nano NFO. In which, the sol–gel auto combustion method is a unique combination of the combustion and the chemical gelation processes. This method, exploiting the advantages of cheap precursors and simple route of preparation, results in ultra fine and homogeneous powder.

More information about the importance and superiority of this route to synthesize spinel ferrites can be found elsewhere [14,15]. Spinel ferrites, orthoferrites and garnets nanoparticles have been synthesized through this method using different fuels such as tetraformal trisazine (TFTA) and oxalic acid dihydrazide (ODH) by K. C. Patil et al., [15,16].

*Corresponding author. Tel.: +91 431 2503608; fax: +91 431 2500133.
E-mail address: hemalatha@nitt.edu (J. Hemalatha).

0272-8842/$ - see front matter © 2013 Elsevier Ltd and Techna Group S.r.l. All rights reserved.
http://dx.doi.org/10.1016/j.ceramint.2013.09.103

The earlier attempt of the authors to synthesize highly crystalline nickel ferrite nanoparticles through combustion technique using DL-alanine as fuel for the first time is reported elsewhere [9] and influence of fuel on crystallite size, magnetic properties, thermal and functional groups are also discussed. In the present work, authors have explored and reported the significant role of nitric acid (HNO_3), added to the precursor solution in the sol–gel auto combustion process, in controlling the reaction rate and in tailoring the structural, thermal and magnetic properties.

2. Synthesis

All the chemicals, nickel nitrate Ni $(NO_3)_2 \cdot 6H_2O$, iron nitrate Fe $(NO_3)_3 \cdot 9H_2O$ and nitric acid (HNO_3), used in this reaction are of analytical grade and are used as purchased from Merck. Double distilled water is used as solvent whereas DL-Alanine ($C_3H_7NO_2$) is used as the fuel for combustion.

The aqueous homogeneous solutions of nickel nitrate and iron nitrate are mixed in 1:2 ratio and stirred for half an hour. Appropriate amount of nitric acid is added to the above solution to enhance the complete dilution and also the reaction rate. Then 2 M of aqueous DL-alanine solution chosen as optimum molarity as suggested in our previous report [9], is added slowly, drop by drop during stirring and the solution is further continuously stirred for 2 h and heated to 80 °C. The solution turned into a viscous gel after complete evaporation of aqueous media and started igniting automatically by yielding voluminous gases while burning. All the by-products of the reaction exist in gaseous state leaving behind NFO in a dark brown fluffy form. The acquired final fluffy product is ground into fine powder and it is annealed at 500 and 800 °C for 2 h. The same procedure is adopted to synthesis more NFO samples by varying the concentration of HNO_3 from 0 to 6 mol/L (0, 2, 5, and 6 mol/L) in order to study the effect of nitric acid on the size and properties of nickel ferrite. The mixing of nitric acid to the precursor solution has the following advantages: 1. NO_3^- ions present in nitric acid form an oxidizing environment and hence increase the rate of oxidation. 2. The number of oxygen vacancies is decreased, and thus, the super exchange interaction of Fe–O–Fe atoms is enhanced [17]. For all the samples the ratio of nickel nitrate: iron nitrate: fuel is maintained to be 1:2:2. The sample codes given for the samples prepared at various conditions are listed in Table 1.

2.1. Characterization

The crystalline structure, phase composition and crystallite size of as-prepared and annealed NFO samples are identified and calculated from XRD patterns obtained using Cu K_α radiation ($\lambda = 1.541$ Å) for 2θ value ranging from 10° to 80° in X-Ray Diffractometer (Rigaku Ultima III). The micrographs of the sample are recorded using electron microscopes (SEM) S-3000H and (TEM) CM200 PHILIPHS. The thermal stability, weight loss and Curie temperature of the samples are investigated in the presence of small magnetic field with a help of TG-DTA(SII TG/DTA 6200 EXSTAR) by heating the samples from 30° to 900 °C with the heating rate of 40 °C/min in nitrogen atmosphere with flow rate of 100 ml/min. The magnetic properties of samples are studied at room temperature using a Vibrating Sample Magnetometer (Lake Shore, USA, Model 7404) with 16.5 KOe as maximum applied magnetic field.

Table 1
Crystal structural parameters.

Sample	Sample code	Crystallite Size nm	Lattice constant Å	dx gm/cm^3	d_A Å	d_B Å
0 mol/L						
As prepared	S1	30.80	8.33	5.391	3.606	2.944
500 °C/2 h	S2	26.00	8.32	5.412	3.602	2.941
800 °C/2 h	S3	32.35	8.31	5.434	3.597	2.937
2 mol/L						
As prepared	S4	10.67	8.31	5.416	3.601	2.940
500 °C/2 h	S5	17.35	8.29	5.472	3.588	2.930
800 °C/2 h	S6	21.40	8.27	5.508	3.580	2.923
5 mol/L						
As prepared	S7	34.50	8.33	5.387	3.607	2.945
500 °C/2 h	S8	35.32	8.33	5.387	3.607	2.945
800 °C/2 h	S9	35.02	8.31	5.426	3.598	2.938
6 mol/L						
As prepared	S10	40.95	8.33	5.389	3.607	2.945
500 °C/2 h	S11	35.95	8.28	5.489	3.584	2.927
800 °C/2 h	S12	40.45	8.31	5.435	3.596	2.936

3. Results and discussion

3.1. Structural studies

The XRD patterns of the as-prepared and annealed NFO samples are shown in Fig. 1. The reflection peaks are indexed with the help of JCPDS No 86-2267 to be (111), (220), (311), (222), (400), (422), (511), (440), (620), (533) and (622) planes which are characteristic of nickel ferrite exhibiting a cubic spinel structure. The peaks becoming sharper and narrower with increase of annealing temperature indicates the improvement of crystallinity with heat treatment. The asprepared sample (S1) synthesized without nitric acid has secondary peaks corresponding to ε-Fe_2O_3, β-Fe_2O_3, and Fe_3O_4. When it is annealed at high temperatures (S2 and S3) the secondary peaks tend to disappear but still retaining a small impurity peak indicating a trace of β-Fe_2O_3. XRD patterns of the samples (S4–S12), prepared with higher concentrations of HNO_3 given in Fig. 1(b–d), have no secondary peaks even when left unannealed. This observation suggests that the addition of HNO_3 with the reactants ensures the phase purity of NFO samples without subjecting them to any heat treatment for further purification.

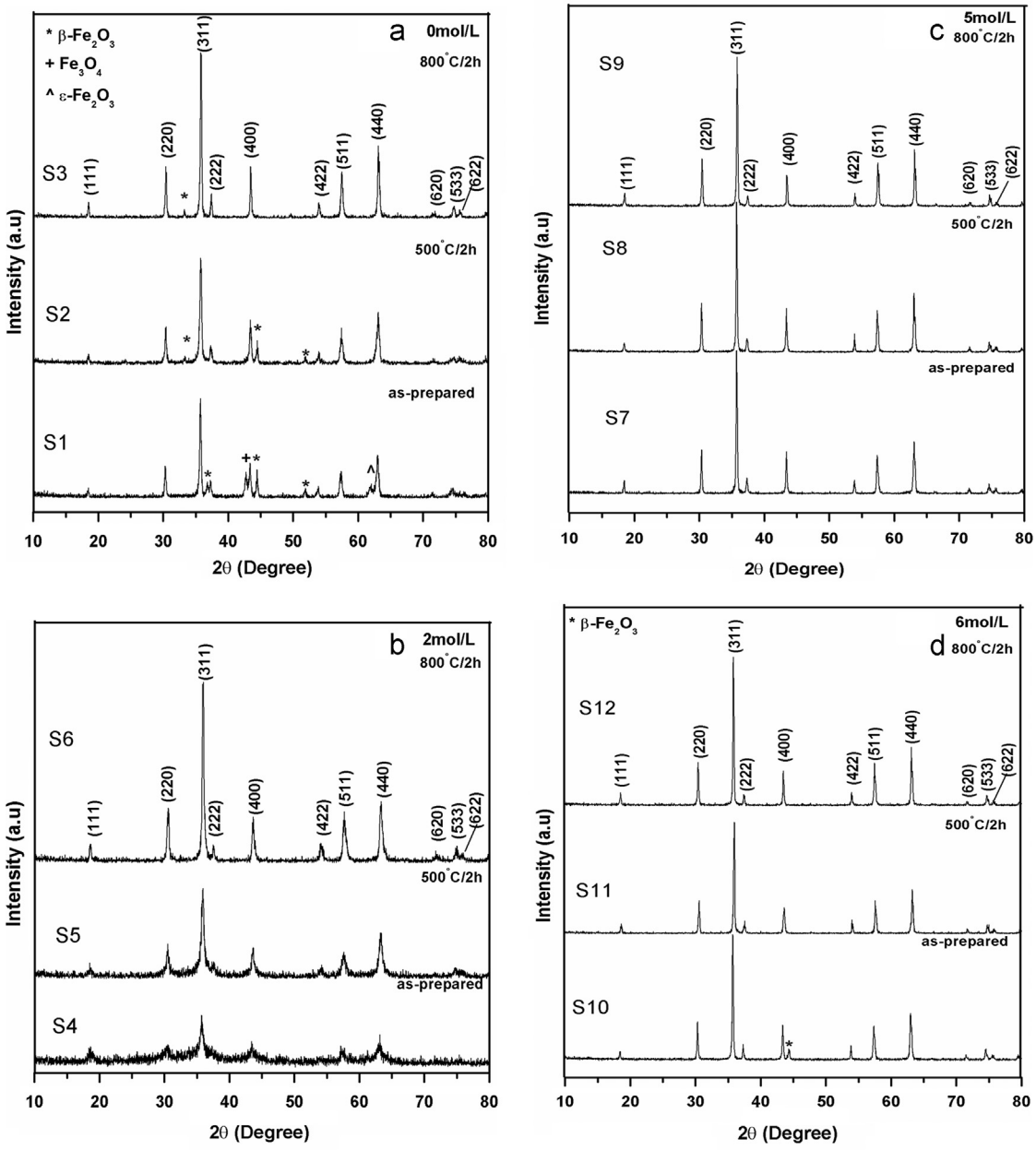

Fig. 1. XRD patterns of NFO samples prepared with various concentrations of HNO_3.

The average crystallite size, lattice constant, theoretical density, and hopping length are calculated as follows and the values are summerized in Table 1.

The average crystallite size is obtained by using Debye Scherrer equation [4].

$$D = \frac{0.9\lambda}{\beta_{hkl} cos\theta} \tag{1}$$

where β_{hkl} is full width at half maximum of the diffraction peak, λ is wavelength of X-ray and θ is Bragg angle. The instrumental corrected broadening, (β_{hkl}) corresponding to each diffraction peak of nanocrystalline $NiFe_2O_4$ are estimated using the following relation [18].

$$(\beta_{hkl})^2 = (\beta_{hkl})^2 measured - (\beta_{hkl})^2 instrumental \tag{2}$$

The lattice constants of all the samples are calculated using the following relation [4]

$$a = d_{khl}\sqrt{h^2+k^2+l^2} \tag{3}$$

where, d_{khl} is interplanar distance. Theoretical density dx of the samples is obtained from the X-ray diffraction data using the equation [4],

$$d_x = \frac{8M}{Na^3} \tag{4}$$

where, M is molecular weight of the sample, N is Avogadro's number. The hopping length between the magnetic ions (the distance between the magnetic ions) in the tetrahedral (A) site and in the octahedral [B] site are calculated from the following

relations [19],

$$d_A = 0.25a\sqrt{3} \quad (5)$$

$$d_B = 0.25a\sqrt{2} \quad (6)$$

where, d_A is hopping length for tetrahedral site and d_B is hopping length for octahedral site.

3.1.1. Effect of annealing temperature

It is known that the variation in annealing temperature can lead to increase or decrease in particle size depending on the method of preparation and reactants concentrations [20]. Table 1 displays a decrease in crystallite size of the samples at 500 °C and then an increase of crystallite size at 800 °C. As-prepared NFO nanoparticles are in the form of fluffy loose powder and have few percentage of porosity. When the sample is annealed at 500 °C the volatile substances are removed, creating more porosity. Increase in porosity reduces the average crystallite size of NFO nanoparticles [21]. But at higher temperature of 800 °C, the smaller grains coalesce to produce larger crystallite size thus decreases the porosity. Also, at higher temperature the activation energy essential for the nucleation is lowered which enhances the crystallite growth [22,23]. In contrary, the sample S4 demonstrates only a growth in crystallite size with annealing temperature and this behavior can be attributed to its smaller size and amorphous nature.

The values of lattice constant listed in Table 1 are comparable to the values 8.34 Å and 8.33 Å reported for nano NFO and bulk NFO respectively [9,24]. The annealed samples have low values because, during annealing more Fe^{2+} ions are transformed into Fe^{3+} ions in octahedral [B] sites by an oxidation process. This process decreases the lattice parameter, since the radius of Fe^{3+} is 0.64 Å and that of Fe^{2+} is 0.74 Å [24]. The increase of theoretical density (dx) with respect to the annealing temperature is observed from Table 1. The reason being the force generated during the thermal treatment drives the grain boundaries to grow over the pores, decreases the pore volume and makes the material denser [25]. Samples S7, S8 and S10 have the theoritical density of 5.38 g/cm^3 which is comparable to 5.37 g/cm^3 that is reported earlier [26] for nano NFO prepared through combustion using urea as fuel. As the lattice parameter decreases, the hopping lengths between the magnetic ions d_A and d_B also decrease with increase of annealing temperature [27] indicating that the magnetic ions come closer to each other.

3.1.2. Effect of nitric acid

Fig. 2 shows an interesting result that, the concentration of nitric acid added with the precursor during the synthesis of nickel ferrite has appreciable influence on the growth of crystallite. The crystallite size is found to be maximum for the samples treated with higher concentration of HNO_3 and is found to be minimum for those treated with low concentration of HNO_3. This can be explained as follows: The particle size is mainly influenced by two factors: (i) nucleation (ii) particle growth and agglomeration. Nucleation in the reaction is instantaneous that starts creating the nuclei when the nitrate solutions are added. When the nuclei density is more the collision between them lead to more agglomeration and it will increase the ultimate equilibrium particle size [28]. As it is

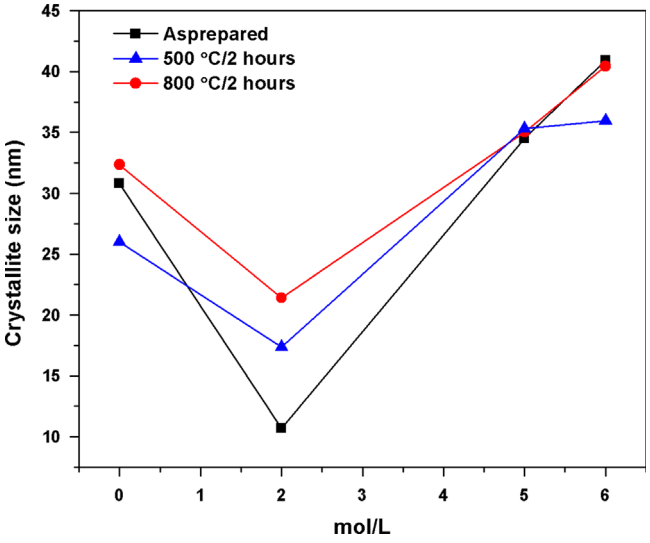

Fig. 2. Variation of crystallite size with increase of HNO_3 concentration.

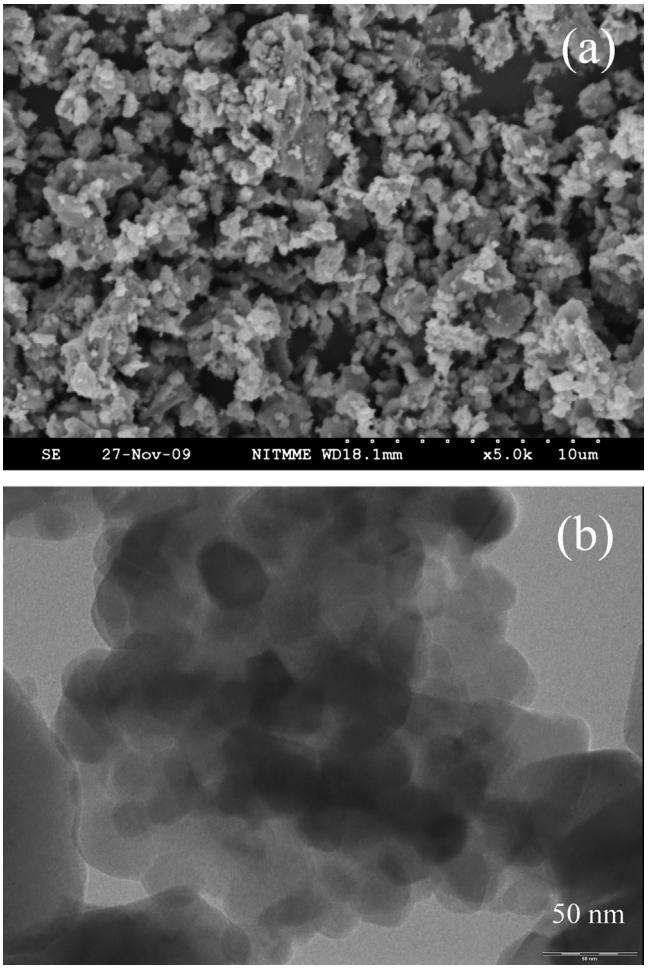

Fig. 3. Electron microscope images of the agglomerates using (a) SEM and (b) TEM.

known, the rate of reaction depends on both the reactant and acid concentrations.

In the present work, as the reactant concentration is maintained constant, the rate of the reaction changes mainly with respect to the HNO_3 concentration. Nitric acid is a strong acid with high ionization constant (Ka), hence it provides high ionic strength to the solution that enhances the reaction rate which in turn quickens the nucleation process. The addition of HNO_3 in low concentration (2 mol/L) increases the ionic strength in the reaction environment and consequently changes the nucleation rate creating huge number of nuclei. At low concentration, the growth process is less complicated, [29] starts shortly after the start of nucleation, that the particle growth and formation of primary and secondary ion layers are resulted around them. Hence, the crystallite size of samples with 2 mol/L become very less and shows amorphous nature. With increase of HNO_3 concentration (5 and 6 mol/L) the reaction rate of both nucleation and growth increases. Consequently, a high speed creation of nuclei and rapid growth of particle take place simultaneously. The small cores stick to larger particles thereby increasing the size.

There is no significant change observed in the lattice parameter values of the samples with the variation of nitric acid concentration. Hence, there is no significant change in other crystallite parameters such as dx, d_A and d_B also with respect to concentrations of HNO_3.

3.2. Morphological analysis

The morphology of samples S7 and S9 determined through SEM and TEM respectively are shown in Fig. 3. SEM image of S7 (Fig. 3a) reveals the agglomeration of particles which can be ascribed to the heat released from combustion. Due to the heat generated during combustion reaction there is not only the formation of agglomeration but also sintering of small particles is observed.

Table 2
Magnetic properties of nickel ferrite.

Sample code	Crystallite size (nm)	M_s (emu/g)	H_c (Oe)	M_r (emu/g)	R_s	Bohr magneton (μB)
S1	30.80	39.55	167.64	08.80	0.22	1.66
S2	26.00	43.65	240.05	11.85	0.27	1.83
S3	32.35	43.03	126.90	07.15	0.17	1.81
S4	10.67	06.81	93.43	00.63	0.09	0.29
S5	17.35	27.01	94.71	02.55	0.09	1.13
S6	21.40	27.02	162.35	04.52	0.17	1.13
S7	34.50	40.40	136.12	09.58	0.24	1.70
S8	35.32	46.20	134.20	09.64	0.21	1.94
S9	35.02	42.47	112.35	07.92	0.19	1.78
S10	40.95	46.78	121.71	11.10	0.24	1.94
S11	35.95	47.29	145.90	11.11	0.24	1.98
S12	40.45	43.52	124.52	07.17	0.16	1.83

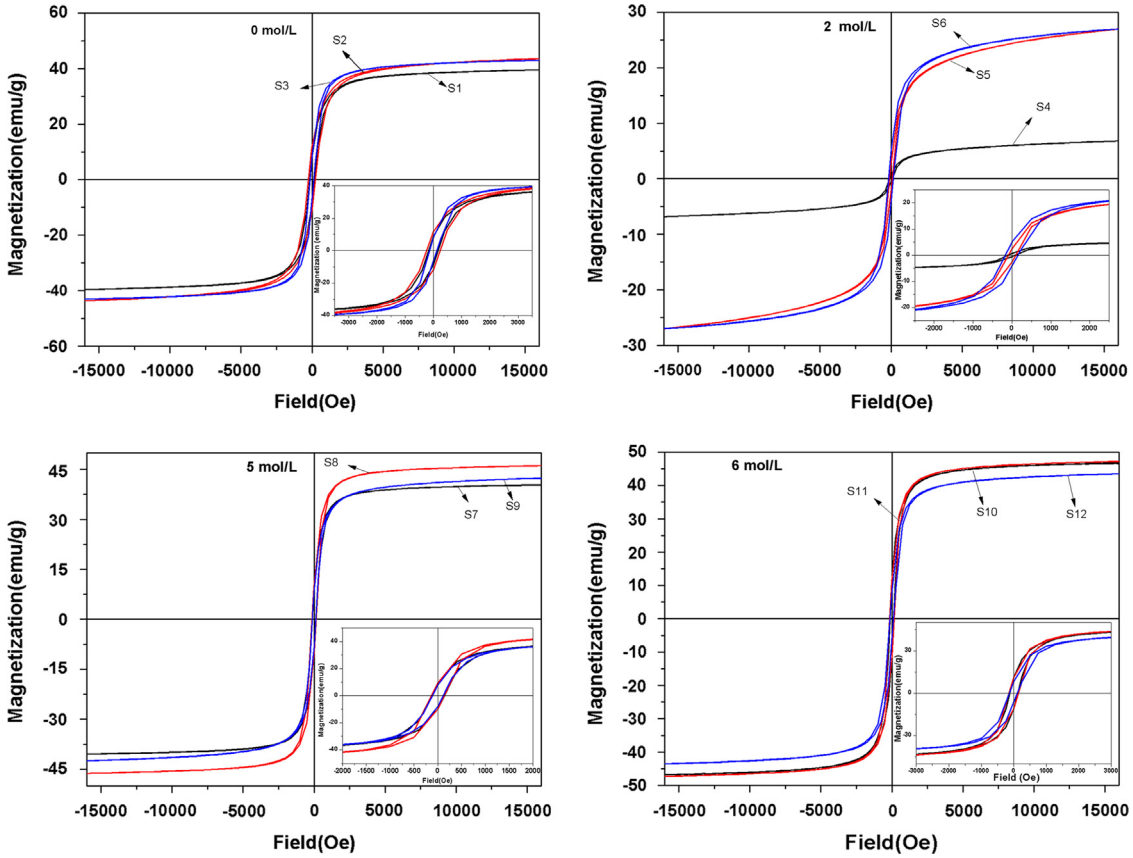

Fig. 4. Room temperature hysteresis loops of NFO samples S1–S12, and low field hysteresis as inset.

In TEM picture of S9 (Fig. 3b), the aggregates which are roughly spherical in shape and non-uniform in size are identified. The average size of those aggregates are found to be 39.6 nm that it is comparable to the value 35 nm calculated from X- ray diffraction details.

3.3. Magnetic properties

The magnetic hysteresis loops of the nickel ferrite samples obtained at room temperature are shown in Fig. 4 and the inset of the Fig. 4 shows the magnified images. The magnetization behavior of the samples are of typical ferrimagnets which can be explained on the basis of changes in exchange interaction between tetrahedral and octahedral sub-lattices. However in nano particles of ferrites there is interplay of four factors namely super-exchange interaction, magneto crystalline anisotropy, canting effect and dipolar interactions between the projected moments on the surface [9]. The saturation magnetization (M_s), coercivity (H_c), remanence (M_r), are given in Table 2.

The magnetic moment (μB) per atom in Bohr magneton for each sample is calculated using the following equation [30], and included in Table 2.

$$\mu_B = M \times \frac{M_S}{5585} \tag{7}$$

where, M is molecular weight of $NiFe_2O_4$. As the magnetization measurements can be fully ascribed to the particle size effects the saturation magnetization, coercivity and remanence are plotted as the function of crystallite size in Fig. 5. An increase of M_s and M_r values with the increase of crystallite size is observed. For the case of coercivity, the values (H_c) increases up to 21.4 nm then decrease for higher crystallite size. The increase of M_s and coercivity can be explained as the results of the grain growth and improved crystallinity. The reducing trend of these plots observed for the bigger crystallites can be ascribed to the pinning defects incorporated into the nanocrystallites, due to lattice mismatch between the intergrowing nanocrystallites when the size increases with annealing process [31]. The bigger crystallites are obtained through high reaction rates maintained during the synthesis or through annealing after the synthesis. Both the processes can affect the crystalline order creating the magneto crystalline anisotropy that can reduce the magnetization effects.

The saturation magnetization of sample S4 with crystallite size of 10.7 nm is 6.81 emu/g and the M_s of sample S11 with crystallite size of 36 nm is 47.3 emu/g which is higher than 46.2 emu/g, M_s value reported for nickel ferrite earlier by the authors. And also, the M_s values obtained through this method is significantly higher than the method proposed by M.G. Naseri et al. [32] and it is less than the value reported by Dehong Che et al. [33].

Squareness ratio is given by the equation [34],

$$R_S = \frac{M_r}{M_S} \tag{8}$$

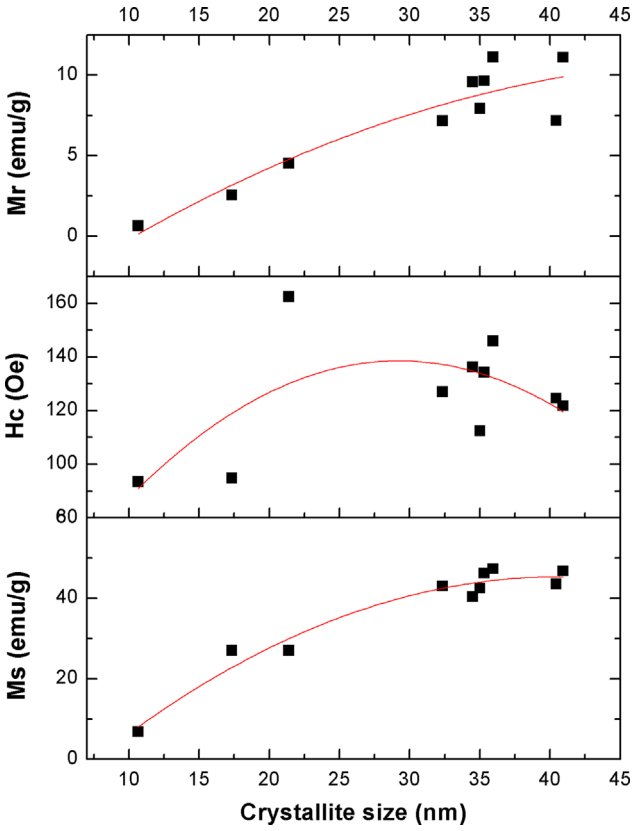

Fig. 5. Variation of magnetic parameters with crystallite size of NFO samples.

It has been reported that the squareness ratio at or above 0.5 indicates that the material is in single magnetic domain and below 0.5 can be attributed to the formation of multidomain structure [34]. The calculated value of squareness ratio of the samples are below 0.5 clearly says that the nickel ferrite nanoparticles synthesized through this method are multidomain in nature. Bohr magneton (μ_B) of the synthesized sample is less than the calculated theoretical value 2 μB for $NiFe_2O_4$. This deviation may be due to from the fact that smaller inversion degree in the obtained material. The negative B–B interaction takes place with antiferrimagnetic coupling between pairs of similar atoms (Fe^{3+} and Fe^{2+}) and with ferromagnetic coupling between non-similar atoms [27].

3.4. Thermal analysis

To find out the Curie temperature of soft ferrites thermo gravimetric analysis has been made in the presence of magnetic field which is applied from the bottom of the pans. While the sample is subjected to temperature scanning near the Curie temperature, as the susceptibility increases, the sample and hence the pan is attracted more towards the field resulting in the weight gain and then drops suddenly above the Curie temperature.

The samples S1, S3, S4, S6, S7, S9, S10, and S12 are subjected to such thermo gravimetric analysis and the thermal curves are shown in Fig. 6. The weight loss and gain observed in percentage with respective of temperature are given in Table 3 for clear observation and discussion. Curie

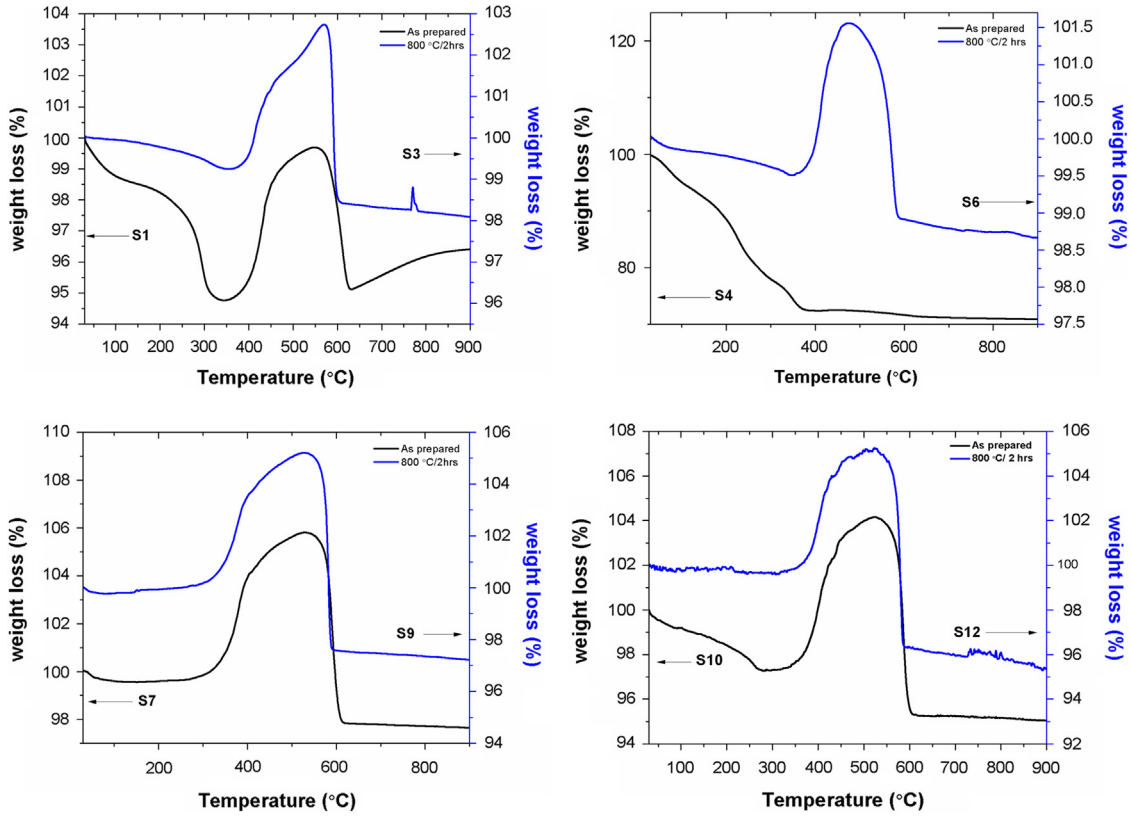

Fig. 6. TG traces of nano NFO samples.

temperatures T_c at which the samples undergo paramagnetic transition also are found and included in Table 3.

Thermograph of sample S1 shows five step weight loss in which first step is observed in the temperature range of 30 °C to 143 °C which is due to the removal of water molecules. Second step weight loss is observed from 144 °C to 343 °C and is ascribed to the loss of residual fuel [9].

In third step of thermograph, there is an anomalous weight gain of 4.94% in the range of 344 °C to 548 °C and in the fourth step there is a sudden weight loss of 4.59% in the range of 549 °C to 631 °C, resulting in the Hopkinson peak [35] which can be explained as follows: The susceptibility $\chi \alpha M_s/\sqrt{K_1}$, where M_s is the saturation magnetization and K_1 is the magnetic anisotropy constant, of the magnetic sample increases with increase of temperature. When the temperature approaches to the Curie point the decrease in rate of crystalline anisotropy constant K_1 is much faster than that of the magnetization M_s and the peak appears when $K_1 \rightarrow 0$ and hence the susceptibility reaches the maximum and suddenly drops to very low value as the material undergoes paramagnetic transition [35] and it gives the curie temperature of the sample. A small weight gain of 1% from 600 to 900 °C is observed which can be attributed to the magnetic transition of the impurities [36] whose presence are indentified through XRD studies.

The annealed sample S3 also shows five step weight loss with the first loss from 30 to 356 °C which is due to the removal of the very few amount of fuel residue present in the sample. The second step of 3.49% weight gain in 357 to 570 °C and third step of 4% weight loss in 570 to 605 °C are due to Hopkinson effect. The peak appearing at 770 °C indicates the Curie temperature of the trace of ε-Fe_2O_3 present in the sample whose existence is proved by XRD pattern (Fig. 1a) [37].

The thermograph of S4 also shows five step weight loss similar to S1 except that Hopkinson peak is missing in S4. From the XRD pattern of sample S4 it is clear that it is more amorphous with small crystallite size of 10 nm. The temperature dependence of the amorphous magnetic anisotropy near the Curie point is quite different from that of the crystalline anisotropy and its rate of decrease is not faster than that of M_s. Hence, there is no Hopkinson peak observed.

The sample S6 shows five step weight loss in which first step is observed in the range of temperature from 30 to 83 °C with a 0.14% loss and weight loss of 0.36% in the temperature of 84 to 347 °C is due to removal of fuel residue. The Hopkinson effect is also observed in S6 with a weight gain of 2.05% in the range of temperature 348 to 475 °C as third step and it gives the curie temperature as 484 °C. In fourth step, sudden weight loss of 2.6% is observed between 476 to 589 °C similar to S3. Rest of the samples S7, S9, S10 and S12 have similar pattern of thermographs with slightly different percentage of weight loss and gain for which the above mentioned explanations are quite valid.

Table 3
Weight loss and gain observed in TGA curves during different stages of transformation.

Sample	Steps	Temperature range (°C)	Weight Loss (%)	Weight gain (%)	T_c (°C)	Assignment
S1	1	30 to 143	0.46	–	562	Removal of O–H molecules
	2	144 to 343	3.78	–	–	Removal of residue fuel
	3	344 to 548	–	4.94	–	Hopkinson peak
	4	549 to 631	4.59	–	–	Ferro to Paramagnetic transition
	5	632 to 900	–	1.32	–	Transition of Impurities
S3	1	30 to 356	0.75	–	578	Removal of residue
	2	357 to 570	–	3.49	–	Hopkinson peak
	3	570 to 605	4	–	–	Ferro to Paramagnetic transition
	4	606 to 900	0.37	–	–	–
	5	765 to 782	–	0.55	–	Curie temperature of Fe
S4	1	30 to 91	5	–	–	Removal of H_2O molecules
	2	92 to 290	17	–	–	Removal of residue fuel
	3	291 to 374	6	–	–	Excess residue and nitrates
	4	468 to 621	1	–	–	–
	5	622 to 900	0.55	–	–	–
S6	1	30 to 83	0.14	–	484	Removal of residue molecules
	2	84 to 347	0.36	–	–	Removal of residue fuel
	3	348 to 475	–	2.05	–	Hopkinson peak
	4	476 to 589	2.6	–	–	Ferro to Paramagnetic transition
	5	590 to 900	0.23	–	–	–
S7	1	30 to 109	0.5	–	562	Removal of H_2O molecules
	2	111 to 254	–	0.06	–	Removal of residue fuel
	3	256 to 530	–	4.37	–	Hopkinson peak
	4	531 to 619	7.2	–		Ferro to Paramagnetic transition
	5	620 to 900	0.19	–		–
S9	1	30 to 96	0.23	–	558	Removal residue molecules
	2	151 to 529	–	5.3		Hopkinson peak
	3	530 to 599	7.62	–	–	Ferro to Paramagnetic transition
	4	600 to 900	0.38	–	–	–
S10	1	30 to 274	2.68	–	558	Removal H_2O and residue
	2	289 to 525	–	6.85	–	Hopkinson peak
	3	526 to 608	8.83	–	–	Ferro to Paramagnetic transition
	4	623 to 900	0.22	–	–	–
S12	1	30 to 300	0.5	–	550	Removal H_2O and residue
	2	302 to 526	–	5.6	–	Hopkinson peak
	3	527 to 590	8.89	–	–	Ferro to Paramagnetic transition
	4	591 to 900	1.01	–	–	–

For all the samples annealed at 800 °C for 2 h (S3, S6, S9 and S12) the percentage of weight loss is observed to be less which proves the high degree of crystallinity of $NiFe_2O_4$ [38]. It is noteworthy that the Curie temperature of the samples varies with the preparation conditions and with the crystallite size.

A plot of Curie temperature versus crystallite size is shown in Fig. 7 which displays an increasing trend of T_c with increase of crystallite size up to around 32 nm but a decreasing trend for higher crystallite sizes. The sample S6 of crystallite size of 21.4 nm has lower Curie temperature of 484 °C whereas the sample S3 with crystallite size of 32.4 nm has high Curie temperature of 578 °C that is comparable to the bulk value 590 °C reported [39]. This dependence of T_c on the crystallite size can be explained on the basis of the molecular field of ferrimagnetism theory [22,40]. According to this theory, as the temperature is raised, magnetization decreases monotonically until it becomes zero at the Curie temperature. The smaller the

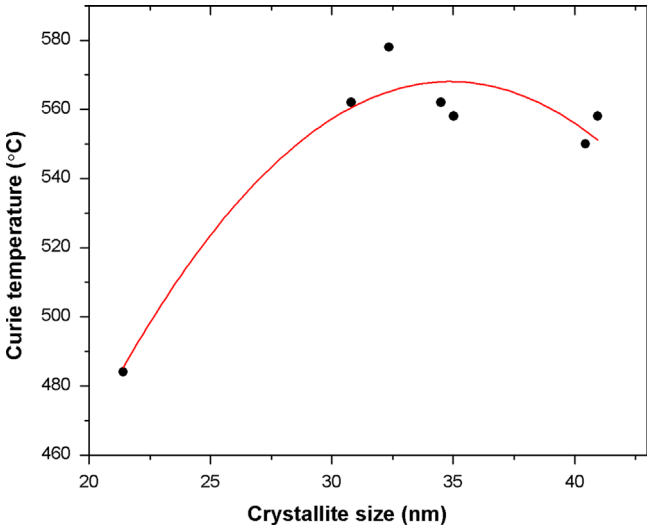

Fig. 7. Variation of Curie temperature with crystallite size.

magnetic particle size, lower is the saturation magnetization, hence lower is the Curie temperature. Also, the surface to volume ratio of smaller partilces is very high and have a significant fraction of atoms on the surface and their (A–O–B) exchange interaction should be weaker because of the lower coordination and hence they will have a reduced average Curie temperature compared to that of interior atoms. This will account for the decrease in Curie temperature [36]. The crystallites of size above 32 nm the M_s value reduces with the increase of crystallite size (Ref. Fig. 5) due to the pinning defects and the lattice mismatch that is explained in the previous section. Hence reduction of M_s value results in the reduction of Curie temperature.

4. Conclusions

Sol–gel auto combustion synthesis of nano-sized nickel ferrite is made in the presence of HNO_3 to demonstrate the effects of nitric acid on crystallinity, crystallite growth, phase purity, thermal and magnetic properties of nanosized nickel ferrite. The XRD patterns reveal the formation of cubic spinel structure of all nano nickel ferrite samples. The addition of 2 mol/L of HNO_3 to the precursor results in the formation of NFO of reduced size of 11 nm whereas the same process conducted without HNO_3 yielded NFO of size 31 nm. It further, provides phase pure samples, removing the impurity phases which exist when prepared without HNO_3. Higher concentrations of HNO_3 added to the precursor solution resulted in the formation of NFO of size ranging from 35 nm to 41 nm. This explains that the addition of HNO_3 influences the reaction rate in such a way that at low concentrations the nucleation process is enhanced and at higher concentrations both the nucleation and growth are enhanced together. Also, it is found that HNO_3 added in low concentration results in amorphous samples. The corresponding changes in the size of the crystallites and crystallinity with respect to the annealing temperature are also discussed. The saturation magnetization of the sample S11 has 47.3 emu/g that is higher than the value reported previously. The TG traces of the crystalline samples show Hopkinson peaks at Curie temperature which occurs as a result of the anomalous increase in susceptibility of the material due to the faster decreasing rate of magnetic crystalline anisotropy constant when compared to the rate of increase of saturation magnetization. The sample S3 has T_c of 578 °C is very close to that of bulk nickel ferrite. Further, the size dependence of the structural, thermal and magnetic parameters has been investigated.

And hence, it is proved that the addition of nitric acid to the reactants is playing a major role in controlling the size, crystallinity, phase purity, thermal and magnetic properties of nickel ferrite. Also, this study proves the possibility to prepare single phase ferrite by carefully controlling the process conditions without subjecting it to any high temperature annealing.

Acknowledgments

The authors acknowledge the DST, Government of India for the TG/DTA facility under the DST Project (SR/FTP/ETA-11/08) and thank Dr. R. Justin Joseyphus, Assistant Professor, NIT, Tiruchirappalli for extending the instrumentation facility for thermal characterization. The authors acknowledge the DST, Government of India for the VSM facility under the FIST programme sanctioned to the Department of Physics, NIT, Tiruchirappalli.

References

[1] M. Salavati-Niasari, F. Davar, T. Mahmoudi, A simple route to synthesize nanocrystalline nickel ferrite ($NiFe_2O_4$) in the presence of octanoic acid as a surfactant, Polyhedron 28 (2009) 1455–1458.
[2] S. Maensiri, C. Masingboon, B. Boonchom, Supapan, A simple route to synthesize nickel ferrite ($NiFe_2O_4$) nanoparticles using egg white, Scripta Materialia 56 (2007) 797–800.
[3] L. Wang, J. Ren, Y. Wang, X. Liu, Y. Wang, Controlled synthesis of magnetic spinel-type nickel ferrite nanoparticles by the interface reaction and hydrothermal crystallization, Journal of Alloys and Compounds 490 (2010) 656–660.
[4] B.D. Cullity, Introduction to Magnetic Materials, Addison–Wesley, Reading, MA, 1972.
[5] M. Srivastava, A.K. Ojha, S. Chaubey, A. Materny, Synthesis and optical characterization of nanocrystalline $NiFe_2O_4$ structures, Journal of Alloys and Compounds 481 (2009) 515–519.
[6] V. Sepelak, I. Bergmann, A. Feldhoff, P. Heitjans, F. Krumeich, D. Menzel, F.J. Litterst, S.J. Campbell, K.D. Becker, Nanocrystalline nickel ferrite, $NiFe_2O_4$: mechanosynthesis, nonequilibrium cation distribution, canted spin arrangement, and magnetic behavior, The Journal of Physical Chemistry C 111 (2007) 5026–5033.
[7] X. Cao, L. Gu, Spindly cobalt ferrite nanocrystals: preparation, characterization and magnetic properties, Nanotechnology 16 (2005) 180–185.
[8] A. Kale, S. Gubbala, R.D.K. Misra, Magnetic behavior of nanocrystalline nickel ferrite synthesized by the reverse micelle technique, Journal of Magnetism and Magnetic Materials 277 (2004) 350–358.
[9] T. Prabhakaran, J. Hemalatha, Combustion synthesis and characterization of highly crystalline single phase nickel ferrite nanoparticles, Journal of Alloys and Compounds 509 (2011) 7071–7077.
[10] J. Huo, M. Wei, Characterization and magnetic properties of nanocrystalline nickel ferrite synthesized by hydrothermal method, Materials Letters 63 (2009) 1183–1184.
[11] H.Z. Wu, G.X. Xia, Effects of synthetic conditions on particle size and magnetic properties of $NiFe_2O_4$, Powder Technology 198 (2010) 157–166.
[12] J.H. Liu, L. Wang, F.S. Li, Magnetic properties and Mössbauer studies of nanosized $NiFe_2O_4$ particles, Journal of Materials Science 40 (2005) 2573–2575.
[13] D. Li, T. Herricks, Y. Xia, Magnetic nanofibers of nickel ferrite prepared by electrospinning, Applied Physics Letters 83 (2003) 4586.
[14] S.A. Seyyed Ebrahimi, J. Azadmanjiri, Evaluation of $NiFe_2O_4$ ferrite nanocrystalline powder synthesized by a sol–gel auto-combustion method, Journal of Non-Crystalline Solids 353 (2007) 802–804.
[15] K.C. Patil, M.S. Hegde, T. Rattan, S.T. Aruna, Chemistry of Nanocrystalline Oxide Materials Combustion Synthesis, Properties and Applications, World Scientific, New Jersey, 2008.
[16] K. Suresh, N.R.S. Kumar, K.C. Patil, A novel combustion synthesis of spinel ferrites, orthoferrites and garnets, Advanced Materials 3 (3) (1991) 148–150.
[17] H. Sozeri, Simple recipe to synthesize single-domain $BaFe_{12}O_{19}$ with high saturation magnetization, Journal of Magnetism and Magnetic Materials 321 (2009) 2717–2722.
[18] V. Biju, N. Sugathan, V. Vrinda, S.L. Salini, Estimation of lattice strain in nanocrystalline silver from X-ray diffraction line broadening, Journal of Materials Science 43 (2008) 1175–1179.
[19] M.A. Amer, M. El Hiti, Mössbauer and X-ray studies for $Ni_{0.2}Zn_xMg_{0.8-x}Fe_2O_4$ ferrites, Journal of Magnetism and Magnetic Materials 234 (2001) 118–125.

[20] M.Z. Dang, D.G. Rancourt, J.E. Dutrizac, G. Lamarche, R. Provencher, Interplay of surface conditions, particle size, stoichiometry, cell parameters, and magnetism in synthetic hematite-like materials, Hyperfne Interactions 117 (1998) 271–319.
[21] A. Faraz, Effect of concentration of Zr^{4+} and Ni^{2+} dopants on electrical, magnetic and Y–K angle of Mg–Cu complex spinel nanoferrites, Journal of Superconductivity and Novel Magnetism 25 (2012) 1055–1063.
[22] G. Nabiyouni, M. Jafari Fesharaki, M. Mozafari, J. Amighian, Characterization and magnetic properties of Nickel ferrite nanoparticles prepared by ball milling technique, Chinese Physics Letters 27 (12) (2010) 126401–126404.
[23] J.H. Ahn, B.T. Ahn, Mechanism of enhanced crystallization of amorphous Si thin films by microwave annealing, Electronic Materials Letters 3 (2) (2007) 69–74.
[24] J. Wang, F. Ren, Ran Yi, A. Yan, G. Qiu, X. Liu, Solvothermal synthesis and magnetic properties of size-controlled nickel ferrite nanoparticles, Journal of Alloys and Compounds 479 (2009) 791–796.
[25] M.L. Rahman, S.T. Mahmud, A.K.M. Akther Hossain, X-ray Studies and Magnetic Properties of Ni–Cu–Zn Ferrite, BARC University Institutional Repository VII (1 and 2) (2010) 9–14.
[26] A.C.F.M. Costa, R.T. Lula, R.H.G.A. Kiminami, L.F.V Gama, A.A. de Jesus, H.M.C. Andrade, Preparation of nanostructured $NiFe_2O_4$ catalysts by combustion reaction, Journal of Materials Science 41 (2006) 4871–4875.
[27] O.M. Hemeda, M.I. Abd El-Ati, Spectral studies of $Co_{0.6}Zn_{0.4}Fe_2O_4$ at different soaking times, Materials Letters 51 (2001) 42–47.
[28] R.G. Chaudhuri, S. Paria, Synthesis of sulfur nanoparticles in aqueous surfactant solutions, Journal of Colloid and Interface Science 343 (2010) 439–446.
[29] A. Elsagh, Synthesis of Silica nanostructures and optimization of their size and morphology by use of changing in synthesis conditions, E-Journal of Chemistry 9 (2) (2012) 659–668.
[30] R.C. Kambale, P.A. Shaikh, S.S. Kamble, Y.D. Kolekar, Effect of cobalt substitution on structural, magnetic and electric properties of nickel ferrite, Journal of Alloys and Compounds 478 (2009) 599–603.
[31] M. Kumar, K.L. Yadav, Magnetoelectric characterization of $xNi_{0.75}$-$Co_{0.25}Fe_2O_4$–$(1-x)BiFeO_3$ nanocomposites, Journal of Physics and Chemistry of Solids 68 (2007) 1791–1795.
[32] M.G. Naseri, E.B. Saion, H.A. Ahangar, M. Hashim, A.H. Shaari, Simple preparation and characterization of nickel ferrite nanocrystals by a thermal treatment method, Powder Technology 212 (2011) 80–88.
[33] Dehong Chen, Dairong Chen, Xiuling Jiao, Yuting Zhao, Maoshuai He, Hydrothermal synthesis and characterization of octahedral nickel ferrite particles, Powder Technology 133 (2003) 247–250.
[34] G. Baldi, D. Bonacchi, C. Innocenti, G. Lorenzi, C. Sangregorio, Cobalt ferrite nanoparticles: the control of the particle size and surface state and their effects on magnetic properties, Journal of Magnetism and Magnetic Materials 311 (2007) 10–16.
[35] B. Boyanov, Synthesis and determination of curie temperature of ferrites from the systems BaO–CoO-ZrO_2–Fe_2O_3 and BaO–NiO–ZrO_2–Fe_2O_3, Journal of Chemical Technology and Metallurgy 41 (1) (2006) 61–64.
[36] C.B. de Boer, M.J. Dekkers, Unusual thermomagnetic behaviour of haematites: neoformation of a highly magnetic spinel phase on heating in air, Geophysical Journal International 144 (2001) 481–494.
[37] A. Aldea, in: V. Barsan (Ed.), Trends in Nanophysics: Theory, Experiment and Technology, Springer, Springer Heidelberg Dordrecht London New York, 2010, p. 294.
[38] D.-H. Chen, X.-R. He, Synthesis of nickel ferrite nanoparticles by so–gel method, Materials Research Bulletin 36 (2001) 1369–1377.
[39] S. Son, M. Taheri, E. Carpenter, V.G. Harris, M.E. McHenry, Synthesis of ferrite and nickel ferrite nanoparticles using radio-frequency thermal plasma torch, Journal of Applied Physics 91 (10) (2002) 7589–7591.
[40] A.H. Morrish, The Physical Principles of Magnetism, JohnWiley and Sons, New York, 1965, p. 264.